Polymer Vol. 39 No. 24 pp. 6021–6036, 1998
0032-3861/98/$ – see front matter

PII: S0032-3861(98)00113-X

Chain conformation and flexibility of thorny rod polymers

Richard A. Vaia[a,*], Doug Dudis[a] and Jacque Henes[b]
[a]*Air Force Research Laboratory, Materials Directorate, Wright-Patterson AFB, Ohio 45433, USA*
[b]*University of Dayton Research Institute, 300 College Park, Dayton, Ohio 45469, USA*
(Received 12 November 1997; revised 22 January 1998; accepted 30 January 1998)

Molecular dynamics simulations and rotational isomeric state (RIS) theory are used to systematically examine the effect of the regioregularity of monomer linkages and the size of the pendant on the rotational barriers, flexibility and chain conformation of substituted polyparaphenylenes including hydrogen, methyl, *tert*-butyl, phenyl, methoyl and benzoyl pendants (R=H, CH_3, $C(CH_3)_3$, C_6H_5, $COCH_3$, and COC_6H_5, respectively). The influence of the substituents on chain structure and properties can be broadly distinguished based on the degree of cooperativity for rotation about the paraphenylene linkage necessitated by the steric demands of the pendant. For some substituents (R=C_6H_5, $COCH_3$, and COC_6H_5), backbone and pendant motion are intimately coupled leading to *thorny rod polymers*. In general, the conformation of these polymers depends on the relative ratio of regiospecific linkages and on the distortions of the backbone bond angles necessary to accommodate the pendants. For example, the persistence length of the chain decreases by almost an order-of-magnitude when the *ortho*-hydrogen of paraphenylene is replaced by a benzoyl pendant. Furthermore, chain flexibility is restricted to specific regioregular linkages and dynamic distortions of the backbone phenyl linkages. The relatively large intramolecular barriers to rotational motion will result in long relaxation times, frustrating chain packing and potentially leading to kinetically limited metastable states in the solid and melt.

(Keywords: thorny rod polymers; polyparaphenylenes; chain conformation and flexibility)

INTRODUCTION

Substituted polyparaphenylenes (SPPPs) consisting of *para*-linked phenyl units with organic substituents randomly distributed along the backbone are emerging as a family of heat-resistant, high-modulus resins with many potential commercial applications[1–19]. The addition of the lateral substituents to the paraphenylene backbone enables increased degrees of polymerization, imparts solubility in common organic solvents and facilitates polymer processing. Recent experimental studies have indicated that these polymers have a surprising degree of conformational flexibility in dilute solution, for example exhibiting persistence lengths that are substantially less than the contour length of the fully extended polymer[14,20]. Other SPPPs, such as ultra-high-molecular-weight poly(benzoyl paraphenylene), are amorphous and exhibit traditional thermoplastic viscoelastic behaviour in the solid state and melt[21,22].

The physical properties of these polymers and the purported architecture of the paraphenylene backbone are intuitively incongruous. Traditionally, paraphenylene polymers are visualized as rigid rods because the linear linkages of the paraphenylene units suggest stiff, highly extended chains. Generally, these rigid-chain conformations lead to highly ordered, crystalline or semi-crystalline materials with a softening temperature in excess of their decomposition temperature. However, recent studies have indicated that *dynamic* (*delocalized*) flexibility may exist along a polyparaphenylene chain[23]. This dynamic flexibility is associated with excitations of the lowest order Rouse modes and imparts a degree of configurational freedom to the SPPPs. This delocalized flexibility may account for the dilute solution behaviour of the chains, but its implication for solid-state properties, such as the amorphous morphology and thermoplastic-like bulk properties of poly(benzoyl paraphenylene) is not obvious *a priori*. Furthermore, a detailed understanding of the interdependence of *delocalized* flexibility (oscillations of the lowest order Rouse modes), *localized* flexibility (energy barriers to bond bending and rotation) and chain architecture (size and extent of lateral substitution) for rigid polymers is incomplete.

In general, atomic-level structural details such as approximate rotational energy barriers, chain conformations, visualization of chain motion and bulk free-volume distribution are difficult to determine experimentally. Techniques such as light scattering, rheometry, small-angle neutron scattering and n.m.r. are often complicated by physical phenomena associated with the extended nature of a rigid rod such as chain aggregation, limited solubilities and non-linear viscoelasticity as well as complex data interpretation and requirements for special isotopically labeled material. As an alternative, simulation techniques such as molecular mechanics/dynamics and Monte Carlo methods have recently been shown to be an effective approach to visualize atomic-level structural details and determine chain flexibility and characteristic parameters[23–35]. These techniques have been successfully applied to a variety of semi-flexible polymers[29–35] as well as rigid

* To whom correspondence should be addressed

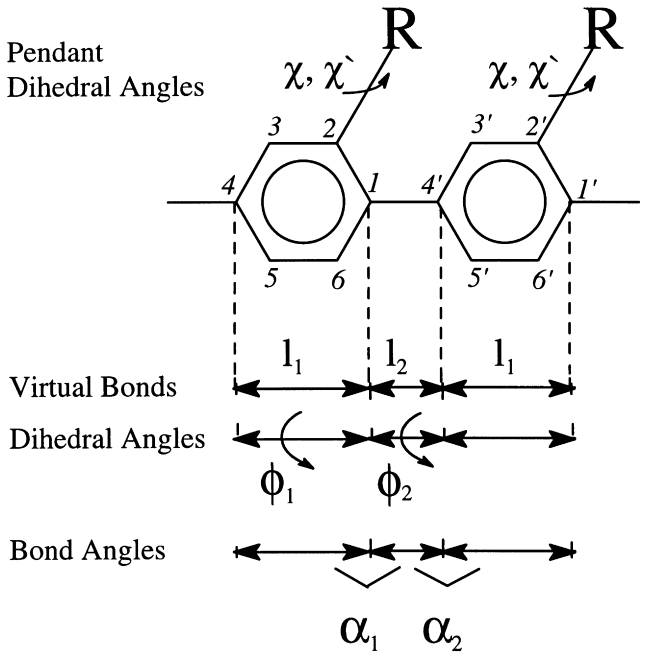

Figure 1 Geometrical parameters for the derivatized polyparaphenylene dimer with a substituent, R. The mer unit is defined as extending from 4 to 4′ carbon. $\boldsymbol{l}_1$ and $\boldsymbol{l}_2$ are virtual bond vectors. α_1 and α_2 are the angles between the bond vectors with and without a pendant *ortho* to the linkage, respectively. ϕ_1 and ϕ_2 are the torsional angles associated with rotation about the backbone virtual bonds. χ corresponds to rotation of the pendant about the initial bond between the pendant and the backbone. χ' corresponds to the internal torsional freedom of the larger pendants. Consistent with previous reports[2], the head (H) of the repeat unit is defined at carbon 1 and the tail (T) is at carbon 4. H–T (depicted above), H–H and T–T mers correspond to 1–4′, 1–1′ and 4–4′ linkages, respectively

polymers, such as polybenzoxazoles[27,28] and polyparaphenylenes[23–26]. Characteristic chain parameters from these studies, such as radius of gyration, persistence length and characteristic ratio, correlate well with the available experimental data.

The objective of this work is to elucidate the relationships between chain architecture, conformation and local flexibility of substituted polyparaphenylenes using molecular mechanics and molecular dynamics modelling and thereby understand the molecular factors underlying the unique physical properties of this class of polymers. We examine a series of paraphenylenes with increasingly large and complex pendants, specifically focusing on poly(benzoyl paraphenylene) because of its great potential as a high-performance thermoplastic resin. Molecular mechanics (MM) calculations are used to systematically examine the effect of substituent size and regioregularity on the rotational barriers and cooperativity within a mer and along the paraphenylene polymer. Molecular dynamics (MD) simulations provide averaged geometric parameters, such as bond lengths and angles, to allow approximation of critical chain parameters such as characteristic ratio, C_∞, and persistence length, a, using rotational isomeric state (RIS) theory. Together, these calculations provide an understanding of the influence of the lateral substituent and regioregularity on the conformation and local flexibility of the polymer chain.

SIMULATION METHODS

Six substituents to a paraphenylene backbone were examined including hydrogen, methyl, *tert*-butyl, phenyl, methoyl and benzoyl (R=H, CH_3, $C(CH_3)_3$, C_6H_5, $COCH_3$, and COC_6H_5, respectively). Geometric parameters for the polymers are defined in *Figure 1*. Because of the asymmetric structure of the monomer, the relative orientation of adjacent monomers produces regiospecificity. Thus three general types of mer linkages can be classified. These are HT–TH, HT–HT and TH–HT where H and T refer to the head or tail of the mer (*Figure 1*), respectively, and the en-dash represents the paraphenyl linkage between the mers. To account for the regiospecificity along the chain, we define the mer unit as containing a backbone phenyl ring and the succeeding linkage, i.e. extending from the 4 to 4′ carbon (*Figure 1*). This effectively gives three types of regiospecific 'mers' that are differentiated by the type of linkage: H–T (T–H), T–T or H–H. Note that in a polymer an H–T or a T–T mer must precede an H–H or an H–T mer and an H–H or a T–H mer must precede a T–T or a T–H mer.

MM calculations and MD simulations were performed using InsightII/Discover 94 v.2.3.7 with the cff91 (Class II) force field[36–38]. The potential energy surface associated with the force field is expressed as:

$$E = E_l + E_\theta + E_\phi + E_{\text{inv}} + E_{\text{cross}} + E_{\text{coul}} + E_{\text{vdW}} \quad (1)$$

where E_l, E_θ and E_ϕ are the bond stretching, bending and torsion terms. E_{inv} represents the improper out-of-plane interactions, E_{cross} includes coupling between bond stretching, bending and torsion, and E_{coul} and E_{vdW} represent non-bonding energy associated with coulombic interactions between electronic partial charges on the atoms and van der Waals interactions, respectively. All non-bonding interactions were considered for structural optimization of the monomers and dimers, whereas a 1.9 nm cutoff based on group atom assignments was used for the MD simulation of oligomers. All MD and MM calculations were performed within a simulated vacuum (dielectric constant, $\varepsilon = 1$) and the contribution of coulombic interactions to the potential energy of the configurations was less than 2% for non-carbonyl-containing moieties and ~10% for carbonyl-containing moieties.

Minimum energy configurations for the three types of mers (H–T, T–T or H–H) were determined based on structural optimization of a dimer. Assuming the configuration of a mer is independent of its neighbours, the dimer contains the essential intramolecular interactions across the paraphenyl linkage. For H–T and T–T mers, the backbone (ϕ) and pendant (χ) dihedral angles were constrained at 6° increments over 360° and the structure was relaxed with molecular mechanics to an energy change of less than 10^{-3} kcal per step. For H–H mers, the additional degree of freedom associated with the second pendant required larger torsional increments (backbone torsion (ϕ) increments at 12° steps from 0° to 180° and pendent torsions (χ_1 and χ_2) increments at 20° steps over 360°). Except for the imposed torsional angle, the initial coordinates of the atoms coincided with the previously minimized structure. Because the internal degrees of freedom of the pendant were not randomized before each structural minimization, the calculated equilibrium configurations reflect a slight memory of the trajectory through potential energy space. As the pendant complexity increases, the relative potential energy of like configurations on the same potential energy surface or configurations determined from different trajectories varied (0% for R=H; <2% for R=CH_3 and $C(CH_3)_3$; and 2–5% for R=$COCH_3$ and COC_6H_5). Note that these are within the uncertainty ($\pm$ 0.1 kcal mol^{-1}) of

estimating the potential energy minima from the potential energy surfaces.

Molecular dynamics trajectories were calculated using ABM4 integrator (Adams–Bashforth–Moulton fourth order) to numerically integrate Newton's equations of motion over small finite time steps ($\Delta t = 0.5$ fs). A Boltzmann distribution of initial velocities was assigned randomly to all atoms such that the average kinetic energy of the system corresponded to the chosen temperature. Trajectories were calculated for a canonical ensemble (NVT) using Nosé dynamics to ensure a Boltzmann temperature distribution[39,40].* In general, after pre-annealing the chain at 1000 K for 400 000 steps (200 ps) to randomize the structure, the chain structure was minimized and the trajectories were calculated at 300 K. After 150 000 steps (75 ps), equilibrium (mean temperature and average temperature fluctuation constant) was reached. Configurations were then collected at 0.5 ps intervals for 500 ps (1000 configurations). Statistical analysis of end-to-end distance, bond angles and torsional angles showed minimal to no correlation between neighbouring mers indicating that to a first approximation a mer configuration is independent of its neighbouring configurations. Reproducible structural parameters that were independent of mer location along the chain were obtained for all but the terminal three mers at the chain ends. These mers were not included in the calculations.

ROTATIONAL ISOMERIC STATE CALCULATIONS

For semiflexible and rigid chains, the single chain conformations and characteristic parameters such as persistence length and characteristic ratio can be determined using the simulation results and either a rotational isomeric state (RIS) formalism or the Porod–Krakty worm-like chain model[27,32–35]. Fundamentally, these approaches are not equivalent—where RIS uses localized structural parameters, the worm-like chain uses average parameters associated with an extended portion of the chain or the entire chain. Since the relative orientation of the backbone and pendant yield distinct states, we choose to calculate the characteristic parameters using a weighted RIS formalism. It is important to note that, with increasing rigidity of the chain, small uncertainties in structural parameters result in large uncertainties in the absolute value of the characteristic parameters, irrespective of the model used[41]. Thus these calculations have the greatest benefit in quantifying trends in a series of related structures.

The RIS formalism approximates various characteristic parameters of a polymer by partitioning the polymer backbone into a series of virtual bonds whose relative orientations (bond and dihedral angles) correlate to the energetically favoured arrangements of the polymer backbone[42]. The virtual bonds may correspond directly to individual covalent bonds or entire rigid sections such as rings or fused rings. Additionally, the RIS formalism requires thermodynamic averages of structural parameters over the ensemble. Assuming MD trajectories faithfully sample configurational space, these thermodynamic averages are well approximated by the temporal averages of structural parameters with fluctuations on a time-scale much less than the duration of the trajectory, such as bond length and bond angle fluctuations.

Conformationally dependent properties are calculated based on the mean orientation of the *i*th virtual bond relative to the *j*th virtual bond. The transformation matrices, $\boldsymbol{T}_i$, convert a vector expressed in the local coordinate system of virtual bond $i+1$ into the expression for the same vector in the local coordinate system for virtual bond *i*. The elements of $\boldsymbol{T}_i$ can be formulated from the angles between the virtual bonds, θ_i, and the dihedral angles for rotation about the virtual bonds, ϕ_i.

$$\boldsymbol{T}_i = \begin{bmatrix} -\cos\theta & \sin\theta & 0 \\ -\sin\theta\cos\phi & -\cos\theta\cos\phi & -\sin\phi \\ -\sin\theta\sin\phi & -\cos\theta\cos\phi & \cos\phi \end{bmatrix}_i \quad \text{for } i > 1 \tag{2}$$

If the orientations of all the virtual bonds are independent, the average product of the transformation matrices of the polymer is equal to the product of the average matrices.

$$\langle \boldsymbol{T} \rangle = \langle \boldsymbol{T}_i \boldsymbol{T}_{i+1} \ldots \boldsymbol{T}_{j-1} \rangle = \langle \boldsymbol{T}_i \rangle \langle \boldsymbol{T}_{i+1} \rangle \ldots \langle \boldsymbol{T}_{j-1} \rangle \tag{3}$$

This is a reasonable approximation for rigid units connected by isolated rotatable bonds[42–44]. However, coupling between units requires truncation of equation (3) before the second equal sign.

If the virtual bond angles are also assumed independent of the dihedral angles for the statistically preferred conformations, the average *i*th transformation matrix becomes

$$\langle \boldsymbol{T}_i \rangle = \begin{bmatrix} -\langle \cos\theta_i \rangle & \langle \sin\theta_i \rangle & 0 \\ -\langle \sin\theta_i \rangle \langle \cos\phi_i \rangle & -\langle \cos\theta_i \rangle \langle \cos\phi_i \rangle & -\langle \sin\phi_i \rangle \\ -\langle \sin\theta_i \rangle \langle \sin\phi_i \rangle & -\langle \cos\theta_i \rangle \langle \cos\phi_i \rangle & \langle \cos\phi_i \rangle \end{bmatrix} \quad \text{for } i > 1 \tag{4}$$

Therefore, conformationally dependent properties can be solely expressed as the average sine and cosine of θ_i and ϕ_i. Note that for an arbitrary angle β, $\langle \sin\beta \rangle \neq \sin\langle\beta\rangle$ and $\langle \cos\beta \rangle \neq \cos\langle\beta\rangle$. Thus when possible $\langle \sin\beta \rangle$ and $\langle \cos\beta \rangle$ should be determined directly from the simulations. When the dihedral angles about the virtual bonds are symmetrically distributed about 0° and 180°, $\langle \sin\phi_i \rangle = 0$. If there is also a one-to-one correspondence of states across 0° and 180°, the states are also symmetric about $-90°$ and $+90°$ and $\langle \cos\phi_i \rangle$ also equals 0, greatly simplifying equation (4).

For the SPPPs, the paraphenyl ring and the succeeding C–C bond can be combined to give an effective transformation matrix per mer, $\langle \boldsymbol{T}_i \rangle = \langle \boldsymbol{T_1} \rangle \langle \boldsymbol{T_2} \rangle$ where $\phi = \phi_1 = \phi_2$ and α_1 and α_2 are defined in *Figure 1*. The effective bond length per mer is then $|\boldsymbol{l}_i| = \frac{1}{2}(\langle l_1 \rangle + \langle l_2 \rangle \langle \cos\alpha_1 \rangle) + \frac{1}{2}(\langle l_2 \rangle + \langle l_1 \rangle \langle \cos\alpha_2 \rangle)$. Thus for each regiospecific mer, there will be a unique $\langle \boldsymbol{T}_i \rangle$ and $|\boldsymbol{l}_i|$ for the various possible conformations, η_i.

* Persistent normal mode oscillations were observed during simulations (500 ps) using the cvff and cff91 forcefields and velocity-scaling methods to control the temperature or with time steps greater than 0.5 fs. These normal modes appear to arise from inhomogenous distribution of energy within the polymer associated with insufficient coupling to the constant temperature bath. The amplitude increases as the simulation progresses and depends on the length of the chain. These oscillations are absent with more rigorous integration methods (ABM4) and techniques to couple to the constant temperature bath (Nosé dynamics).

Table 1 Equilibrium structures and torsional barriers for various H–T and T–T regiolinkages

Pendant			Equilibrium angles[a]			Torsional barriers[b]		
R	Conformation[c]	Energy[c] (kcal mol^{-1})	$\|\phi\|$	χ	χ'	ΔE_ϕ (kcal mol^{-1})	ΔE_χ (kcal mol^{-1})	$\Delta E_{\chi'}$ (kcal mol^{-1})
H			40, 140	–	–	1.5, 0.8[d]	–	–
CH_3	T–T		40, 140	–	–	1.5, 0.8[d]	–	–
	H–T		60, 120	0, ± 120	–	8.0	0.5	–
$C(CH_3)_3$	H–T		90	± 60, ± 180	–	15	0.75	–
C_6H_5	H–T		60, 120	± 60, ± 120	–	7.0	7.0	–
$COCH_3$	H–T a_I	0.0	90	180	0, ± 120	8.0	14	2.5
	b_{II}	0.5	90	0	0, ± 120	9.5	14	1.3
COC_6H_5	T–T		40, 140	–	–	2.0, 1.0[d]	–	–
	H–T a_I	0.0	140	150	−20	11	5.5[e] 3.5	13.5
	a'_I	0.2	40	−150	20	11	5.5[e] 3.5	13.5
	b_{II}	2.0	115	−30	−20	12	7.5[e] 4.0	18.0
	b'_{II}	2.2	65	30	20	12	7.5[e] 4.0	18.0

[a]Angles defined such that a *trans* orientation is 180°. All linkages are symmetric about $\phi = 0$. Estimated uncertainty ± 3°
[b]Energy corresponds to the potential energy difference between the energy minimum and saddle-point configurations. Unless otherwise noted, saddle-point configuration is located at $\phi = 0$ or $\chi = 0$. Estimated relative error is ± 0.5 kcal mol^{-1}
[c]Conformations for each pendant are arranged with respect to increasing relative potential energy. Subscripts I and II correspond to the phenyl or methyl part of the pendant extending over the paraphenyl linkage, respectively
[d]Saddle point at $\phi = 90$
[e]Saddle point at $\chi = 80$

The relative probability of the *i*th mer being in the ηth preferred state is expressed through the statistical weight matrix, $\boldsymbol{U}_i$, where

$$\boldsymbol{U}_i = \begin{array}{c} \begin{matrix} \eta_1 & \eta_2 & \cdots & \eta_\nu \end{matrix} \leftarrow \text{state of } i\text{th mer} \\ \begin{matrix} \eta_1 \\ \eta_2 \\ \vdots \\ \eta_\nu \end{matrix} \begin{bmatrix} w_{11} & w_{12} & \cdots & w_{1\nu} \\ w_{21} & \ddots & & \vdots \\ \vdots & & \ddots & \vdots \\ w_{\nu 1} & \cdots & \cdots & w_{\nu\nu} \end{bmatrix} \\ \uparrow \text{ state of } i-1\text{th mer} \end{array} \tag{5}$$

η_ν is the total number of possible states (configurations) for all the regiospecific mers. States with energies greater than 5 kcal mol^{-1} constitute less than 0.03% of the total population at 300 K and are not considered. w_{ij} is the statistical weight associated with an $\eta_i\eta_j$ combination and is proportional to the occupational probability of the $\eta_i\eta_j$ combination. Since the states are defined per mer, $\boldsymbol{U}_i$ is a square matrix. If the state of the $i-1$th and *i*th mer are independent, then w_{ij} represents simply the relative probability of occupancy of state η_i. For regioregular chains with all H–T (or T–H) linkages, each row of $\boldsymbol{U}_i$ is equivalent. For regioregular chains with alternating H–H and T–T linkages, null values must be included in the statistical weight matrix to exclude the possibility of two H–H linkages or two T–T linkages being adjacent. In this case the total number of states per mer is the sum of the number of H–H and T–T states and each row of $\boldsymbol{U}_i$ is not equivalent. For regioirregular chains, all potential H–T, T–H, H–H and T–T states must be considered and null values must be included in $\boldsymbol{U}_i$ to exclude the possibility of structurally impossible linkages. Even though H–T and T–H states are equivalent through symmetry, they must be considered separately to account for all possible combinations of mers along the chain.

From $\boldsymbol{U}_i$ and $\langle \boldsymbol{T}_i \rangle$, various conformationally dependent properties of a chain can be determined using a weight RIS formalism[42]. One important quantity often used to characterize the stiffness of a chain is the characteristic ratio, defined as

$$C_n = \frac{\langle r^2 \rangle_0}{\sum_{i=1}^{n} l_i^2} \tag{6}$$

where $\langle r^2 \rangle_0$ is the mean square end-to-end distance of an unperturbed chain of length, *n*. C_∞ is the limiting value as *n* approaches infinity and is characteristic of the basic chain architecture. For a random flight chain, $C_\infty = 1$, and in all other cases, $C_\infty > 1$. Usually, the greater C_∞ is the more extended and 'stiffer' the chain. Specific details of the calculation of $\langle r^2 \rangle_0$ and C_∞ from $\boldsymbol{U}_i$ and $\langle \boldsymbol{T}_i \rangle$ are included in the Appendix.

Additionally, the persistence length, *a*, can be estimated from the limiting characteristic ratio by

$$a = \langle |\underline{\boldsymbol{l}}| \rangle (C_\infty + 1)/2 \tag{7}$$

where $\underline{\boldsymbol{l}}$ is the effective bond length per mer. This expression eliminates the dependence of the persistence length on the choice of the first virtual bond encountered when calculating *a* directly from $\langle \boldsymbol{T} \rangle$[32,33].

RESULTS

Table 1 summarizes the equilibrium structures determined from MM for various H–T and T–T regiospecific mers. *Figure 2a–e* shows the corresponding potential energy surfaces for rotation about the backbone (ϕ) and about the side group (χ) for H–T mers of R = CH_3, $C(CH_3)_3$, C_6H_5, $COCH_5$ and COC_6H_5, respectively. Estimated minima (+) and saddle points (●) are depicted on the potential energy surfaces. Representative minimum energy and saddle-point structures are also shown in the figures. For clarity, only potential energy contours corresponding to the lowest 10 kcal mol^{-1} are shown. Note that $\phi = 0°$, ± 180° corresponds to a planer orientation of the two backbone phenyl groups.

Potential energy barriers to conformation change (± 0.5 kcal mol^{-1}) can be approximated from the relative energy between the saddle-point and minima in *Figure 2a–e* and are summarized in *Table 1*. Our calculated energy barriers for rotation about an unsubstituted phenyl linkage (ΔE_0 = 1.5 kcal mol^{-1} and ΔE_{90} = 0.8 kcal mol^{-1}) agree favour-

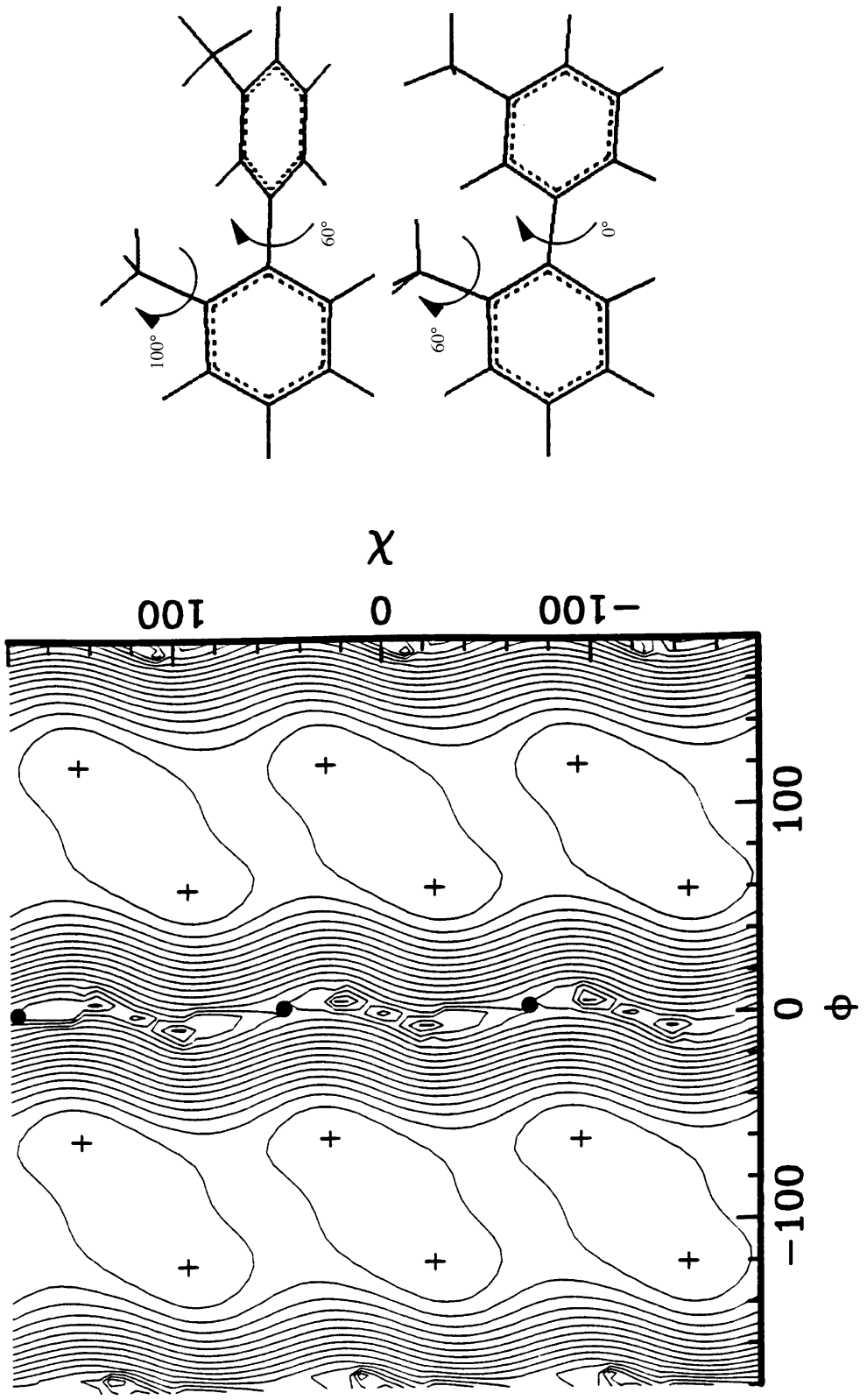

Figure 2 Potential energy surfaces for rotation about the backbone (ϕ) and about the side-group (χ) for H–T dimers. (a) R = CH_3; (b) R = $C(CH_3)_3$; (c) R = C_6H_5; (d) R = $COCH_5$; (e) R = COC_6H_5. Contour spacing is 0.5 kcal mol^{-1} and contours corresponding to the lowest 10 kcal mol^{-1} are shown. '+' and '●' correspond to minima and saddle-points on the potential energy surface, respectively. Representative low-energy and saddle-point configurations are also shown

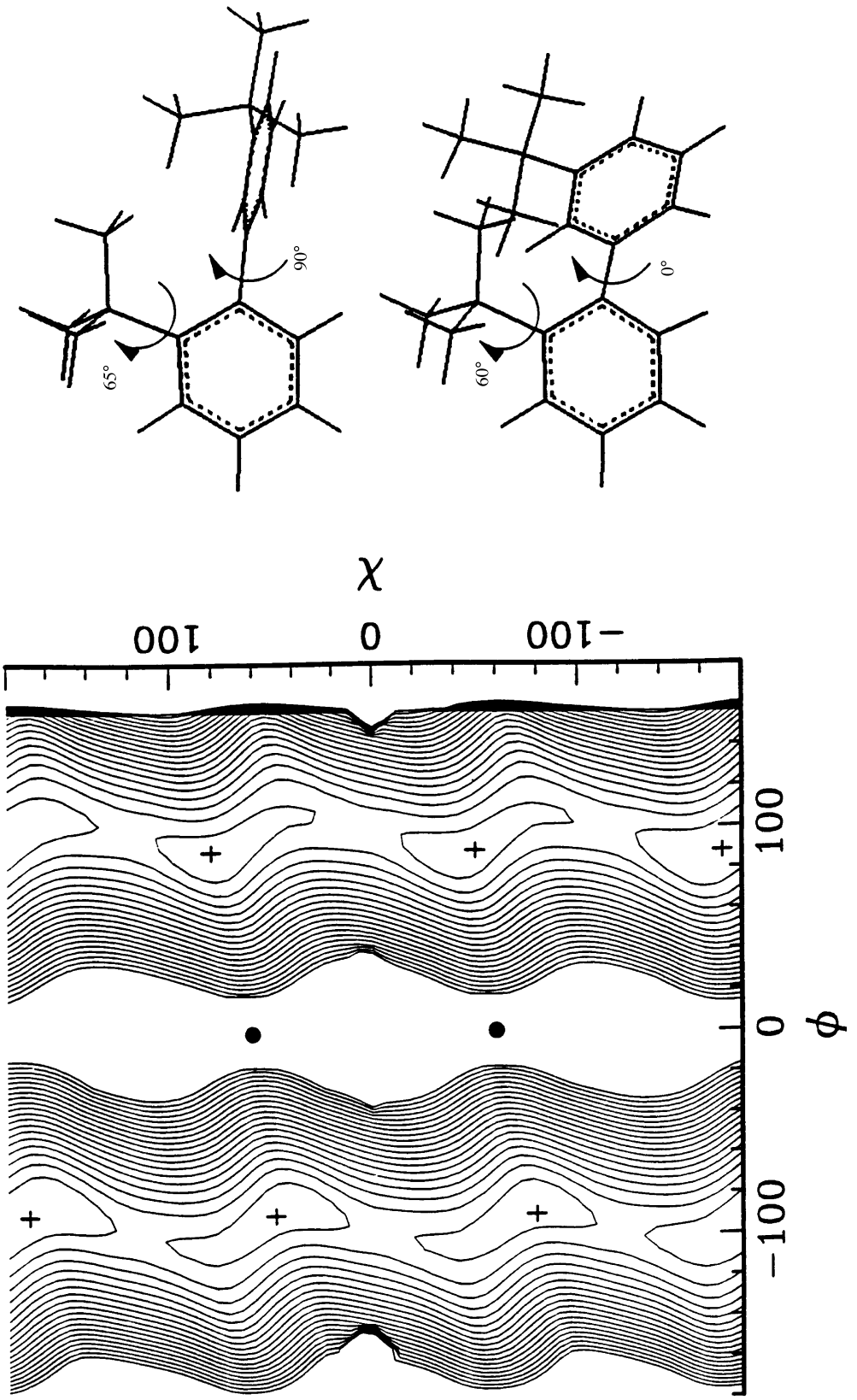

Figure 2 Potential energy surfaces for rotation about the backbone (ϕ) and about the side-group (χ) for H–T dimers. (a) R = CH_3; (b) R = $C(CH_3)_3$; (c) R = C_6H_5; (d) R = $COCH_5$; (e) R = COC_6H_5. Contour spacing is 0.5 kcal mol^{-1} and contours corresponding to the lowest 10 kcal mol^{-1} are shown. '+' and '●' correspond to minima and saddle-points on the potential energy surface, respectively. Representative low-energy and saddle-point configurations are also shown

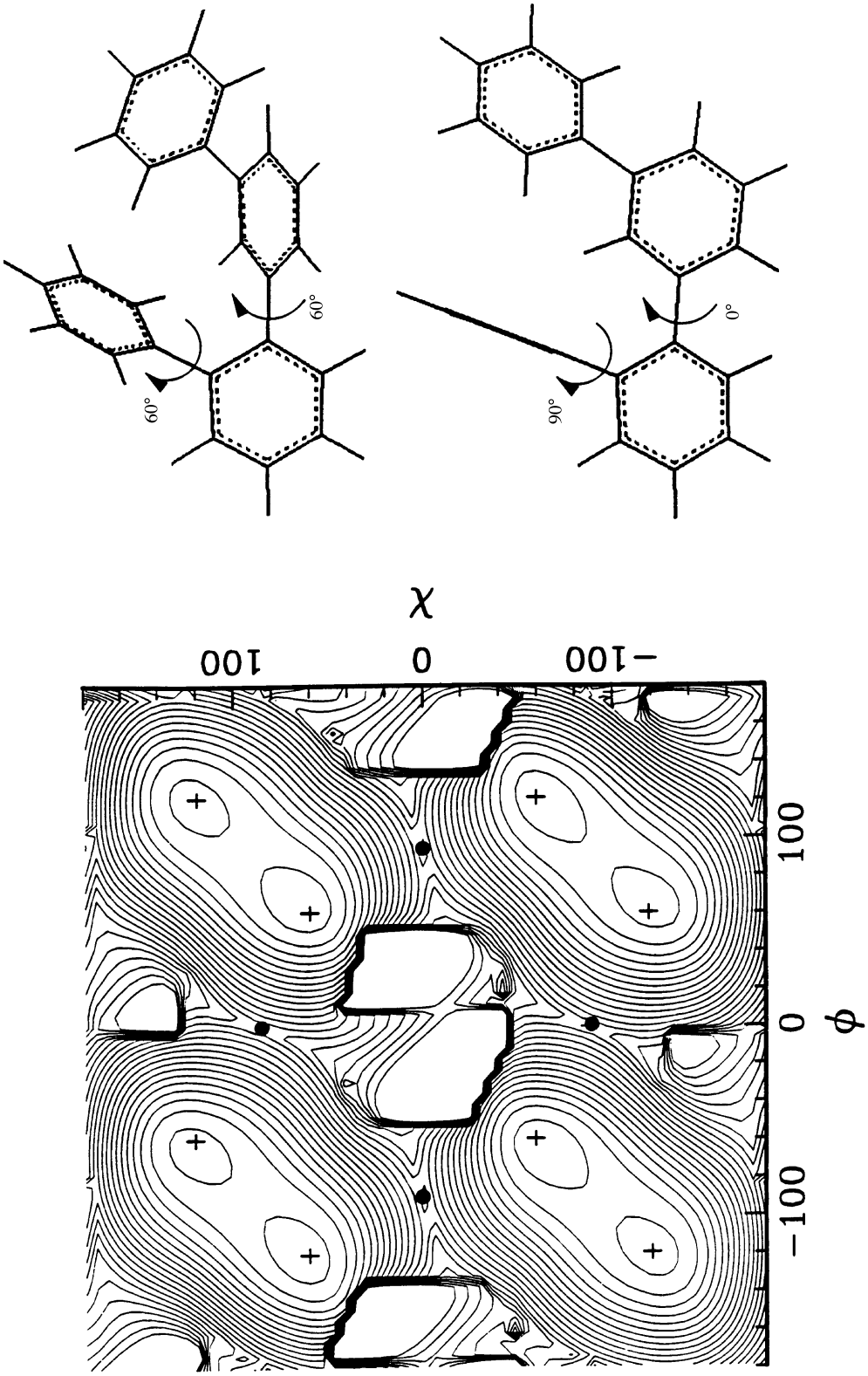

Figure 2 Potential energy surfaces for rotation about the backbone (ϕ) and about the side-group (χ) for H–T dimers. (a) R = CH_3; (b) R = $C(CH_3)_3$; (c) R = C_6H_5; (d) R = $COCH_3$; (e) R = COC_6H_5. Contour spacing is 0.5 kcal mol^{-1} and contours corresponding to the lowest 10 kcal mol^{-1} are shown. '+' and '●' correspond to minima and saddle-points on the potential energy surface, respectively. Representative low-energy and saddle-point configurations are also shown

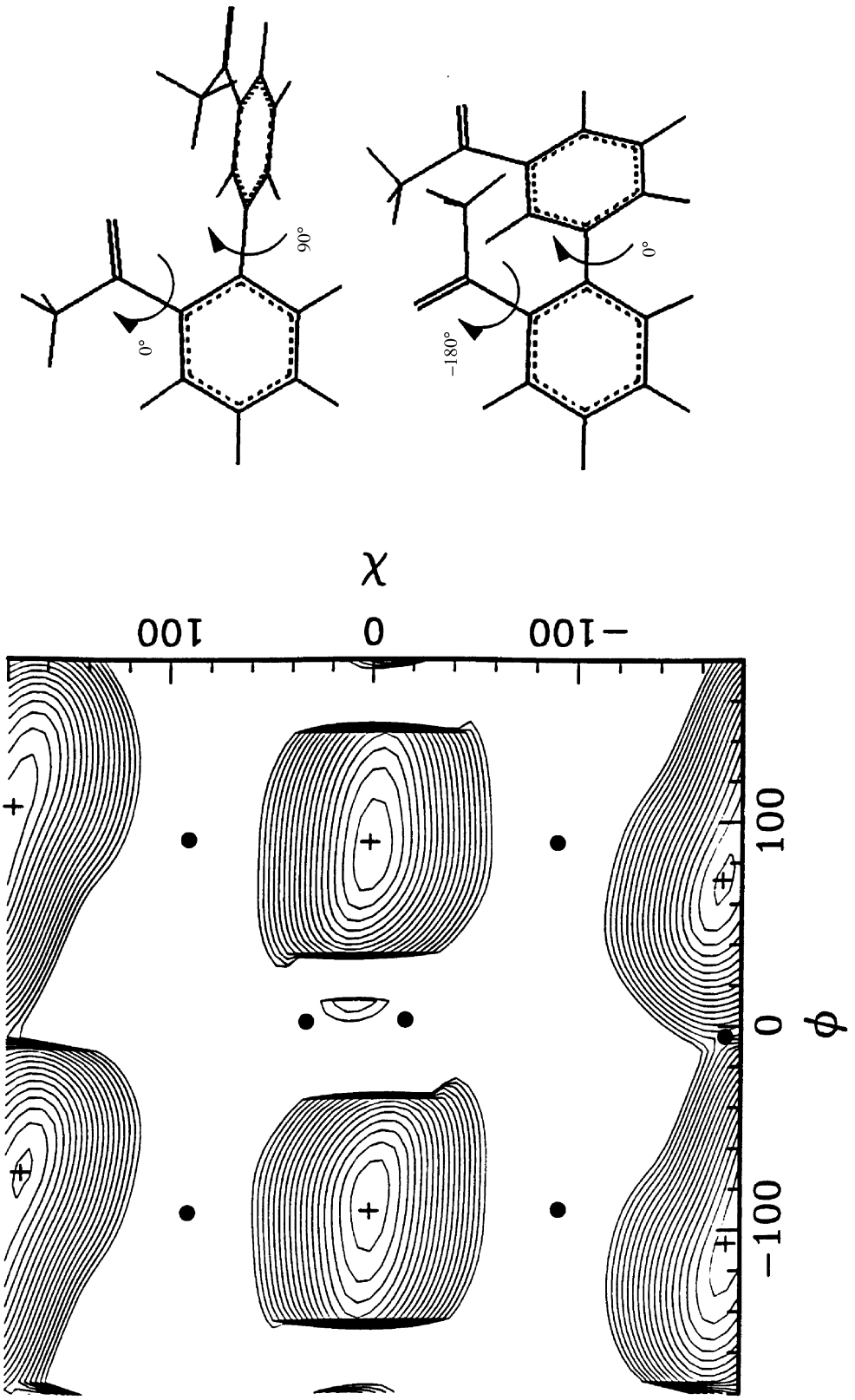

Figure 2 Potential energy surfaces for rotation about the backbone (ϕ) and about the side-group (χ) for H–T dimers. (a) R = CH_3; (b) R = $C(CH_3)_3$; (c) R = C_6H_5; (d) R = $COCH_5$; (e) R = COC_6H_5. Contour spacing is 0.5 kcal mol^{-1} and contours corresponding to the lowest 10 kcal mol^{-1} are shown. '+' and '●' correspond to minima and saddle-points on the potential energy surface, respectively. Representative low-energy and saddle-point configurations are also shown

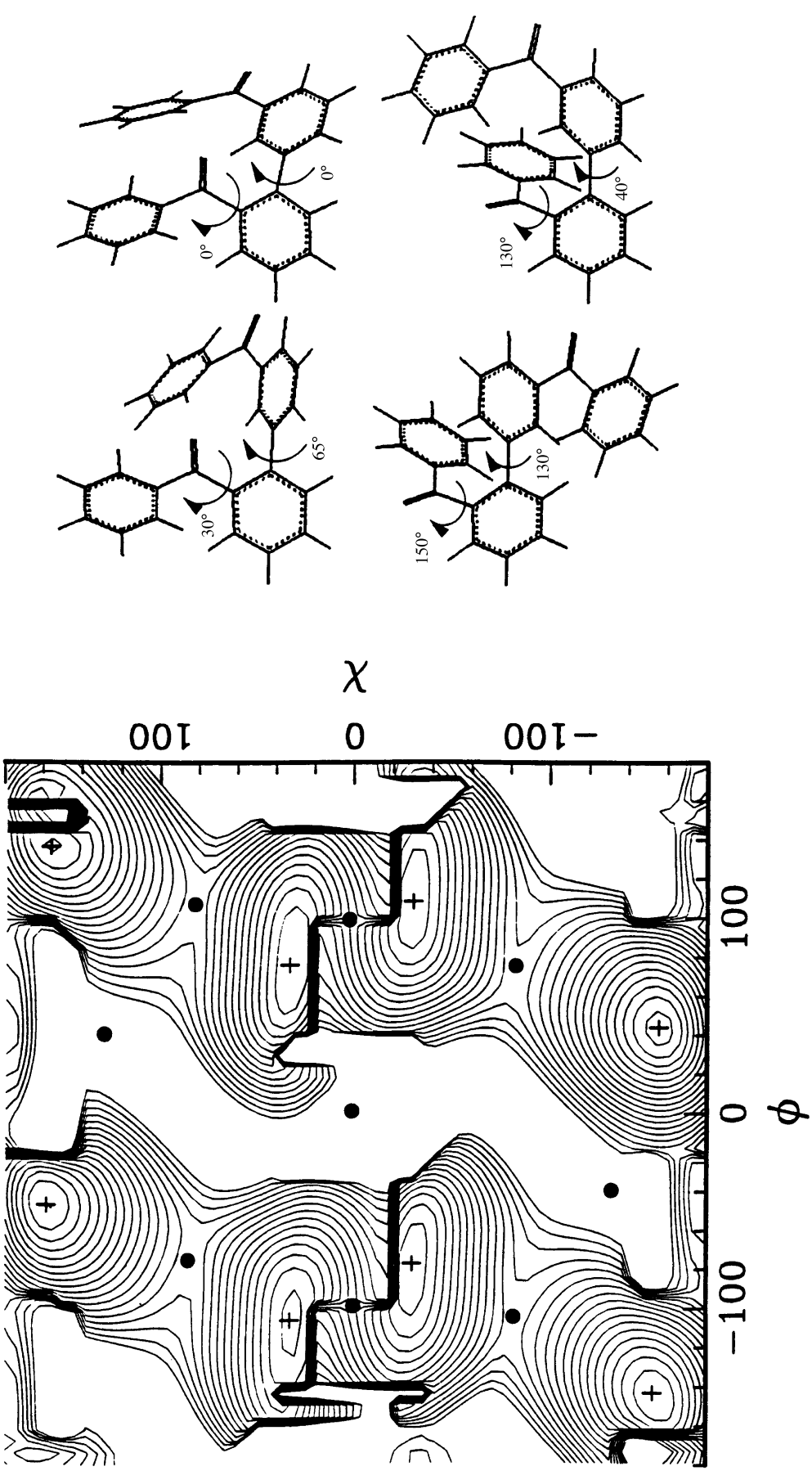

Figure 2 Potential energy surfaces for rotation about the backbone (ϕ) and about the side-group (χ) for H–T dimers. (a) R = CH_3; (b) R = $C(CH_3)_3$; (c) R = C_6H_5; (d) R = $COCH_5$; (e) R = COC_6H_5. Contour spacing is 0.5 kcal mol^{-1} and contours corresponding to the lowest 10 kcal mol^{-1} are shown. '+' and '●' correspond to minima and saddle-points on the potential energy surface, respectively. Representative low-energy and saddle-point configurations are also shown

Table 2 Lowest potential energy structures for various H–H regiolinkages

Pendant			Equilibrium angles[a]				
R	Conformation[b]	Energy[b] (kcal mol^{-1})	$\|\phi\|$	χ_1	χ_2	χ'_1	χ'_2
CH_3	H–H		90	0, ± 120	0, ± 120	–	–
COC_6H_5	H–H a_{II-II}	0.0	60	30	30	20	20
	b_{II-II}	2.0	80	− 30	30	− 20	20
	b_{I-II}	2.0	55	30	− 150	20	20
	b'_{I-II}	2.0	130	− 20	150	− 20	− 20
	c_{II-II}	3.0	95	− 30	− 30	− 20	− 20
	c_{I-II}	3.0	125	25	145	20	− 20
	d_{I-II}	5.0	60	− 15	− 155	− 25	30

[a]Angles are defined such that a *trans* orientation is 180°. All linkages are symmetric about $\phi = 0$. χ_1, χ_2, χ'_1 and χ'_2 correspond to the torsional angles of the pendants. Initial angles were determined from energy minimization and verified by molecular dynamics with an uncertainty of ± 3°
[b]Conformations are arranged with respect to increasing relative potential energy. Subscript I and II correspond to phenyl or carbonyl portions of the pendant extending over the paraphenyl linkage, respectively

ably with previous experimental ($\Delta E_0 = \Delta E_{90} = 1$–2 kcal mol^{-1})[45] and other computational results (MM: 2.1 and 0.9[22]; AM1: 2.2 and 1.0[22]; ab initio: 3.5 and 1.6[45]).

For the carbonyl-containing side-groups (R = $COCH_3$, COC_6H_5), the additional degree of freedom arising from internal rotation of the pendant (χ, χ') leads to two distinct orientations of the pendant—the carbonyl oriented over the paraphenyl ring (subscript I, $90 < |\chi| < 180$) and oriented over the backbone paraphenyl linkage (subscript II, $0 < |\chi| < 90$). Additionally, the potential energy of the configuration depends slightly on the orientation of the neighbouring pendant even though the equilibrium torsion angle is unaffected. Dimer conformations with the pendants on opposite sides of the backbone ($|\phi| > |90|$; a_I, b_{II}) are slightly lower in energy (< 0.2 kcal mol^{-1}) than those with pendants on the same side of the backbone ($|\phi| < 90$; a'_I, b'_{II}). If the second pendant is removed from the dimer (R = COC_6H_5 for the first mer and R = H for the second mer), the primed and unprimed states are equivalent.

Table 2 summarizes the equilibrium structures for H–H linkages of R=CH_3 and R=COC_6H_5. For R=CH_3, perpendicular orientation of the phenyl rings results in a threefold degenerate state of the methyl pendants similar to that observed in the H–T linkage. For R=COC_6H_5, interactions between the pendants greatly restrict their potential orientations. Only II–II and I–II combinations of side-group orientations result in minimum energy configurations that are within ~5 kcal mol^{-1} of the lowest energy configuration, a_{II-II}. The complexity associated with three independent torsional angles hinders the estimation of lowest energy trajectories through saddle points and corresponding potential energy barriers.

Table 3 summarizes the average values and deviations for the kinetic energy, potential energy, temperature and end-to-end distance from the various MD trajectories. In general, the orientation of the mers along the polymers was chosen to provide at least two linkages corresponding to the equilibrium structures summarized in *Tables 1* and *2*. Because Nosé coupling was used to control the temperature of the simulation, the kinetic energy and temperature conform to a normal distribution about ~300 K. For the time-scale of the simulations, torsional motion about the backbone ($\phi = 0°$) was not observed in any chain at 300 K. The only exchanges between structural minima occurred across $\phi = 90°$ in paraphenylene at or beyond the frequency of data collection (2 tHz). In general, because of the large energy barriers to torsional motion in the SPPP systems, insufficient backbone rotation events occur during the MD trajectory to yield statistically significant average dihedral angle. For the length of the simulations, torsional motion with barriers heights greater than 0.5–1 kcal mol^{-1} (*Tables 1* and *2*) were not observed.

Figure 3 shows configurations from the MD trajectories at 200 ps for 15 mer regioregular H–T chains with R = H, CH_3 and COC_6H_5. Throughout the simulations, all the chains remained essentially linear (*Table 3*). In contrast to previous simulations showing large-scale oscillations of end-to-end distance (see p. 6023 footnote), no indication of excitation of these low-order Rouse modes were observed for the simulation conditions chosen. Excitation of the low-order Rouse modes led to bond angles that depended on the fractional position of the bond along the chain. This complicates the determination of average structural parameters and the calculation of chain parameters via RIS methodology.

Tables 4 and *5* summarize the average bond angles and bond lengths and the corresponding distribution for the various minimum energy structures of R=H, CH_3 and COC_6H_5 detailed in *Tables 1* and *2*. These values were determined from at least 2 mers with different neighbour linkages. In general, the average structural parameters agreed within 5% and were independent of the

Table 3 Summary of molecular dynamic trajectories

	Regio-linkages	Mers/chain	Potential energy (kcal)		Kinetic energy (kcal)		Temperature (K)		End-to-end distance (nm)[a]	
			$\overline{PE}$	σ^b_{PE}	$\overline{KE}$	σ^b_{KE}	$\overline{T}$	σ^b_T	$\overline{R}$	σ^b_R
H		15	1682.8	8.1	134.0	8.1	295.9	17.6	6.523	0.010
CH_3	HT	15	1661.3	9.1	174.4	8.9	297.1	15.1	6.461	0.011
	HH, TT	15	1811.5	18.3	174.2	9.5	296.6	16.2	6.472	0.010
COC_6H_5	HT	15	2327.3	11.9	294.9	12.2	298.0	12.3	6.105	0.016
	HH, TT[c]	15	2513.6	21.8	295.5	12.5	298.6	12.6	6.407	0.008
	HH, TT[c]	15	2519.3	21.0	295.5	12.5	298.6	12.6	6.243	0.009
	HT, HH, TT	20	3140.7	13.6	392.5	13.5	297.9	10.2	8.351	0.013

[a]Distance determined from terminal hydrogens
[b]Standard deviation of the data
[c]Initial structure was pre-assigned and the chain structure was minimized

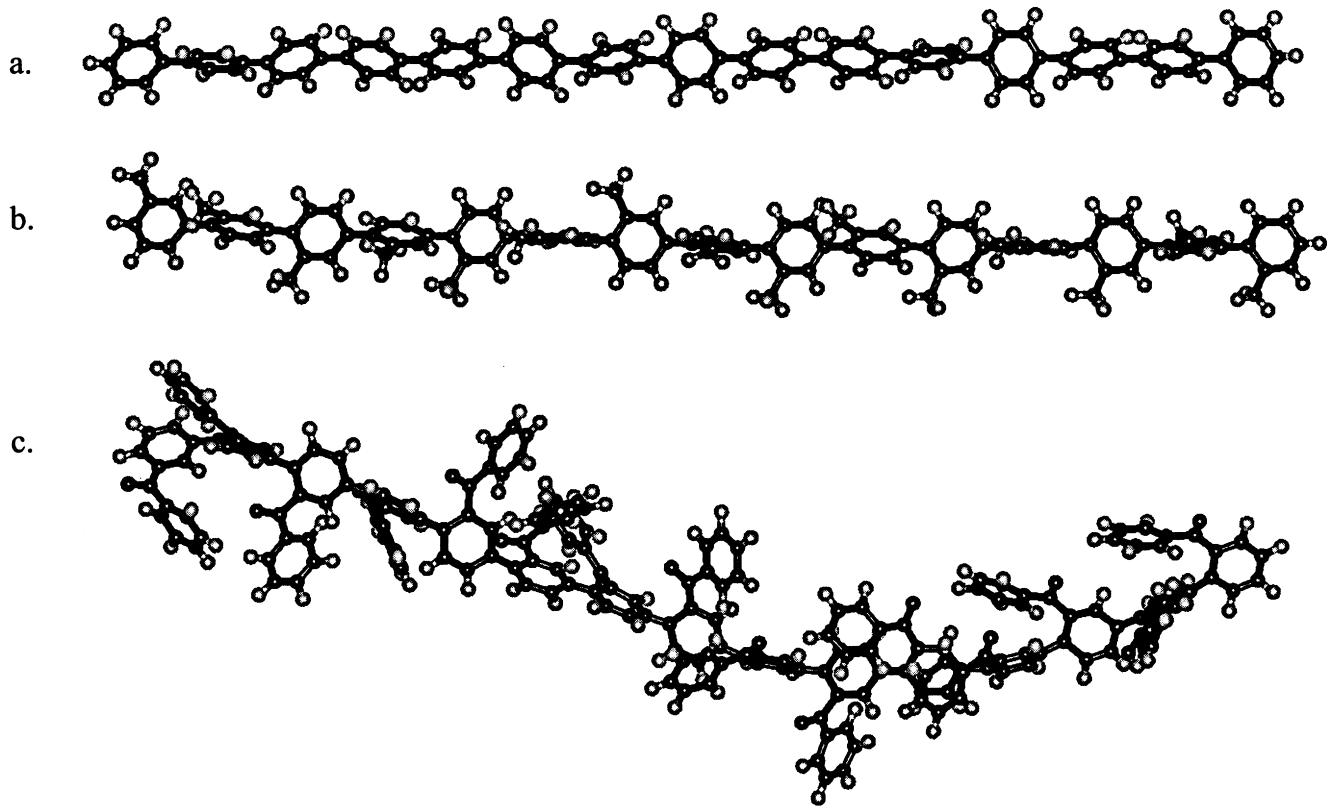

Figure 3 Configurations of 15 mer regioregular H–T chains with; (a) R = H; (b) R = CH_3; (c) R = COC_6H_5

regiospecificity of the surrounding linkages. This implies any intramolecular coupling between pendants on adjacent linkages has at the most a second-order influence on the average chain parameters and that equation (3) is a valid approximation. The one exception is the T–T linkage with R = COC_6H_5. When backbone bending in the neighbouring linkage was greater than 10–12°, the average bond angle for the T–T linkage increased from 3.5° to 9°. Because of the unrestricted environment of the T–T linkage, strain associated with the neighbouring linkage may be relaxed by inducing bending at the adjacent T–T linkage. To conform with the assumption of independent linkages, the average structural parameters for the T–T linkage were determined only from the vast majority of linkages that exhibited MD trajectories similar to the T–T linkages of R = H and CH_3 (*Table 4*).

DISCUSSION

Local molecular structure

The minimum energy configurations of the SPPPs mers are dependent on the size and shape of the pendant and can be clearly seen in the potential energy surfaces (*Figure 2a–e*). In general, the backbone phenyl rings adopt a staggered orientation (*Tables 1* and *2*), even for unsubstituted paraphenylene. For a methyl pendant, the backbone rings are moderately staggered and relatively large areas of configurational space are energetically accessible as

Table 4 Average structural parameters for T–T and H–T regiolinkages of R = H, CH_3 and COC_6H_5

	H	CH_3		COC_6H_5				
		T–T	H–T	T–T	a_I	a'_I	b_{II}	b'_{II}
Bond length (nm)								
$\langle l_1 \rangle$ ($\delta_{l1} = 0.004$[a])	0.292	0.289	0.289	0.289	0.289	0.289	0.289	0.289
$\langle l_2 \rangle$ ($\delta_{l2} = 0.003$[a])	0.139	0.140	0.138	0.141	0.139	0.139	0.139	0.139
$\langle l_0 \rangle$[b]	0.431	0.429	0.426	0.429	0.426	0.425	0.427	0.426
Bond angle								
$\langle \alpha_1 \rangle$	–	–	4.2	–	9.7	16.2	5.9	12.5
$\delta^c_{\alpha 1}$	–	–	5.1	–	7.7	8.3	6.5	7.7
$\langle \cos \alpha_1 \rangle$	–	–	0.9966	–	0.9842	0.9586	0.9935	0.9747
$\langle \sin \alpha_1 \rangle$	–	–	0.0729	–	0.1679	0.2780	0.1032	0.2159
$\langle \alpha_2 \rangle$	3.4	3.5	4.1	(3.8)[d]	5.6	3.7	3.6	4.5
$\delta^c_{\alpha 2}$	4.3	4.3	4.9	(4.7)	6.8	4.8	4.6	5.8
$\langle \cos \alpha_2 \rangle$	0.9977	0.9977	0.9967	(0.9972)	0.9940	0.9973	0.9975	0.9960
$\langle \sin \alpha_2 \rangle$	0.0593	0.0601	0.0711	(0.0660)	0.0980	0.0644	0.0629	0.0791

[a] Standard deviation of bond length fluctuation during MD trajectory

[b] $\langle l_0 \rangle = \frac{1}{2}(\langle l_1 \rangle + \langle l_2 \rangle \langle \cos\theta_1 \rangle) + \frac{1}{2}(\langle l_2 \rangle + \langle l_1 \rangle \langle \cos\theta_2 \rangle)$ where $\theta_1 = \alpha_1$ and $\theta_2 = \alpha_2$ for H–T linkage, $\theta_1 = \alpha_2$ and $\theta_2 = \alpha_2$ for T–T linkage, and $\theta_1 = \alpha_1$ and $\theta_2 = \alpha_1$ for H–H linkage

[c] Full-width-at-half-maximum of the distribution of bond angles during MD trajectory

[d] Depending on nearest neighbour linkage, average bond angle varies. Average restricted to the vast majority of linkages that exhibited MD trajectories similar to the other T–T linkages

Table 5 Average structural parameters for H–H regiolinkages of R = CH_3 and COC_6H_5

	CH_3	COC_6H_5						
		a_{II-II}	b_{II-II}	b_{I-II}	b'_{I-II}	c_{II-II}	c_{I-II}	d_{I-II}
Bond length (nm)								
$\langle l_1 \rangle$ ($\delta_{11} = 0.004$[a])	0.292	0.289	0.289	0.289	0.289	0.289	0.289	0.289
$\langle l_2 \rangle$ ($\delta_{12} = 0.003$[a])	0.140	0.138	0.137	0.139	0.139	0.137	0.139	0.138
$\langle l_0 \rangle$[b]	0.426	0.426	0.425	0.423	0.422	0.425	0.421	0.425
Bond angle								
Side A[c]								
$\langle \alpha_1 \rangle$	3.5	4.5	4.2	7.0	9.4	4.0	6.9	9.1
$\delta^d_{\alpha 1}$	4.3	5.7	4.5	5.5	5.4	4.4	4.8	5.0
$\langle \cos \alpha_1 \rangle$	0.9976	0.9961	0.9968	0.9916	0.9859	0.9971	0.9921	0.9866
$\langle \sin \alpha_1 \rangle$	0.0615	0.0807	0.0732	0.1209	0.1630	0.0691	0.1196	0.1586
Side B[c]								
$\langle \alpha_1 \rangle$ ($\sigma_{\alpha 1}$)	–	4.6	5.1	13.5	14.3	4.1	17.2	7.3
$\delta^d_{\alpha 1}$	–	5.7	5.2	5.8	5.1	4.1	5.5	5.0
$\langle \cos \alpha_1 \rangle$	–	0.9960	0.9954	0.9713	0.9683	0.9970	0.9545	0.9899
$\langle \sin \alpha_1 \rangle$	–	0.0810	0.0891	0.2322	0.2463	0.0716	0.2950	0.1362

[a]Standard deviation of bond length fluctuation during MD trajectory
[b]$\langle l_0 \rangle = \frac{1}{2}(\langle l_1 \rangle + \langle l_2 \rangle \langle \cos\theta_1 \rangle) + \frac{1}{2}(\langle l_2 \rangle + \langle l_1 \rangle \langle \cos\theta_2 \rangle)$ where $\theta_1 = \alpha_1$ and $\theta_2 = \alpha_2$ for H–T linkage, $\theta_1 = \alpha_2$ and $\theta_2 = \alpha_2$ for T–T linkage, and $\theta_1 = \alpha_1$ and $\theta_2 = \alpha_1$ for H–H linkage
[c]Side A and side B refer to the bond angles associated with different pendant orientations. For example, for the conformer b_{I-II}, side A refers to the α_1 angle *ortho* to the I pendant orientation and likewise side B refers to the α_1 angle *ortho* to the II pendant
[d]Full-width-at-half-maximum of the distribution of bond angles during MD trajectory

indicated by the large area within the first two energy contours. As the pendant size increases (*tert*-butyl), the energetically accessible space substantially decreases and backbone dihedral angles are constrained around 90°. For pendants with a more planar shape such as phenyl or benzoyl, the final structure depends critically on the coupling between the orientation of the pendant and the backbone (*Figure 2a–e*) and the extent of accessible configurational space is further reduced. The non-coplanar orientation has been observed in many previous studies and higher-level ab initio calculations[23,26,45]. The stability of the out-of-plane orientation of the backbone rings results from a balance of steric hindrance between the *ortho*-positions

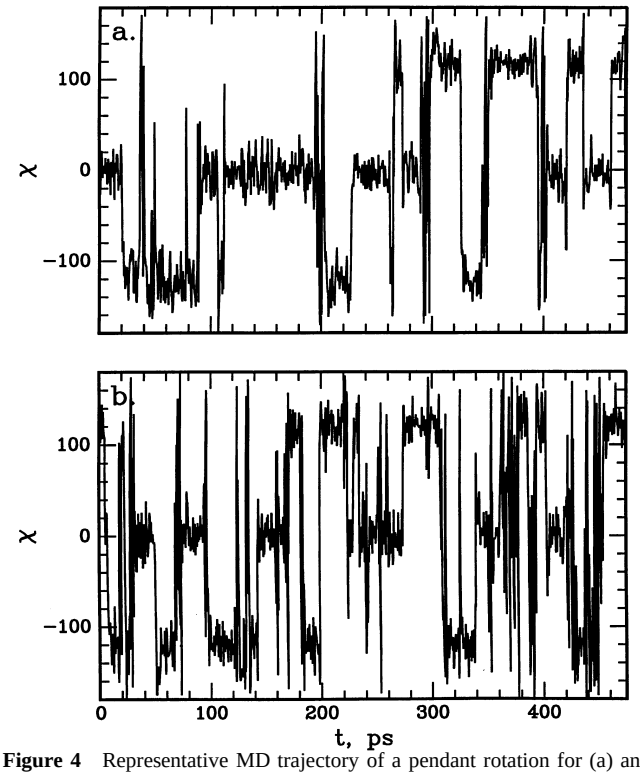

Figure 4 Representative MD trajectory of a pendant rotation for (a) an H–H and (b) an H–T linkage in a 15 mer methyl-substituted polyparaphenylene

which force the rings out of planarity and the electrostatic interaction between the π-orbitals of the phenyl rings which favours increased planarity.

In addition to forcing the backbone phenyl groups out of planarity, steric interactions induce bending of the paraphenyl linkage, observable in both the MM and MD results. The largest distortions are localized at the pendant side of the paraphenylene linkage (α_1) and depend critically on the pendant size and regiospecificity of the linkage (*Figure 2a–e*). For example, no backbone bending ($\alpha_1 = \alpha_2 = 0$) is present for R = H or T–T mers, whereas $\alpha_1 \sim 1$–$2°$ for the methyl pendant, $\alpha_1 \sim 7$–$8°$ for the *tert*-butyl pendant and, depending on the specific ϕ–χ state, α_1 is as large as 10° for the benzoyl group. In comparison, $\alpha_2 \sim 1$–$2°$ for the H–T isomers irrespective of the pendant. The asymmetry of the backbone is also demonstrated in the thermally excited structures observed in the MD simulations (*Tables 4 and 5*).

Previous ab initio calculations indicate that the energetic cost to bend a planar and a 45°-staggered biphenyl 15° out of plane is 2.7 kcal mol^{-1}[22] and 1.5 kcal mol^{-1},[46] respectively. The energy to distort the biphenyl is less than or the same order of magnitude as many of the calculated torsional barriers (*Table 1*). Thus, an SPPP is likely to bend out of plane to reduce the steric repulsion induced by the pendant. This leads to equilibrium configurations where $\alpha > 0$. In contrast to flexible and semi-flexible polymers, where backbone bending is a minor contributor to overall chain flexibility, the distortions arising from the side-groups will have a fundamental influence on the single-chain conformation and flexibility of these 'rigid' chains and thereby also on their bulk properties.

Flexibility and cooperativity

Torsional motion of the backbone is usually considered necessary for non-localized relaxation processes such as occur at the glass transition temperature or during translational diffusion. The dependence of the torsional barriers on pendant size and regiostructure is well known and commonly attributed to the establishment of specific associative interactions or, as in the case studied here, increased steric hindrance between the pendant and backbone moieties. The energetic barriers for torsional motion

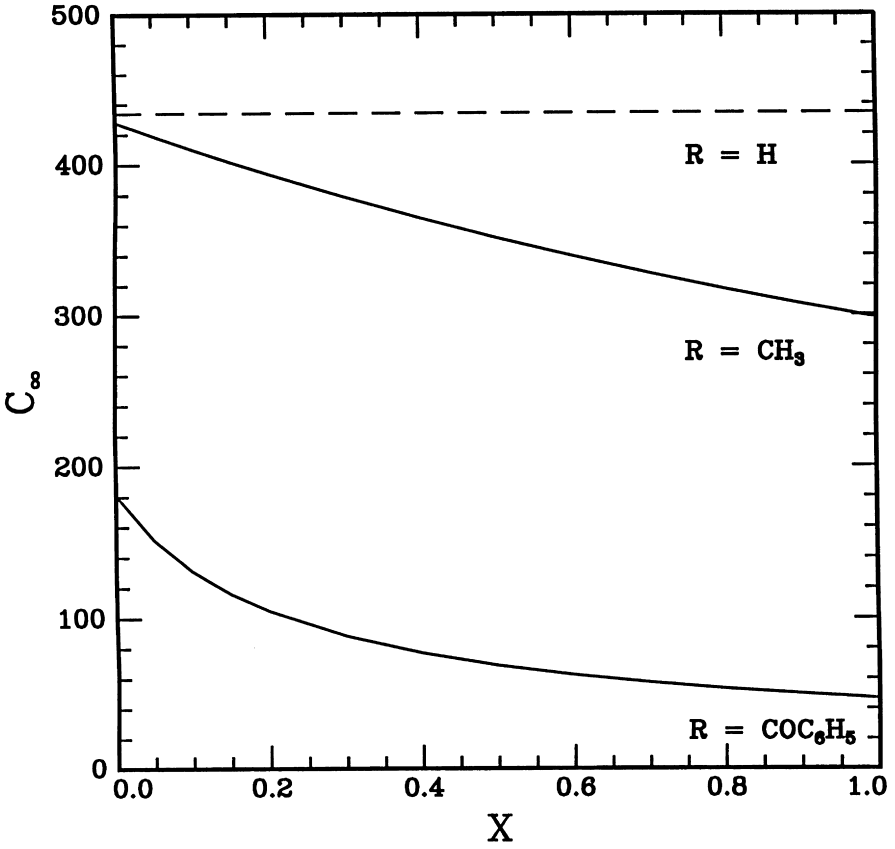

Figure 5 Dependence of C_∞, determined at 300 K, on the relative fraction of H–T linkages, *X*, for methyl-substituted and benzoyl-substituted polyparaphenylene. C_∞ for polyparaphenylene ($C_\infty \sim 434$) is included for comparison (dashed line)

along the chain increase as the size and spatial extent of the pendant increase and are influenced by the regioregularity of the paraphenyl linkages (*Tables 1* and *2*, *Figure 2a–e*). The steric hindrance associated with one (H–T) or two (H–H) pendants substantially increases the barrier for rotation about the paraphenyl linkage relative to the T–T linkage. Note that since the local environment around the backbone T–T linkage is similar to that of biphenyl, the barrier to rotation is approximately equal to that of biphenyl and is independent of the type of pendant. Thus for the larger pendants such as benzoyl, backbone torsional motion will be predominately restricted to T–T conformers. Since the energetic barriers for H–T and H–H motions are substantial, a greater T–T content will increase the flexibility and rotational freedom of these chains.

Two general classes of pendants, A and B, can be differentiated based on their influence on chain motion and local configurational freedom. For class A pendants, steric interactions restrict backbone orientation (ϕ) but the pendant is relatively free to rotate (χ). This occurs for methyl and *tert*-butyl (*Figure 2a,b*) where the trajectories between structural minima are generally dependent only on ϕ or χ. For relatively small potential energy barriers, the independent rotation of the pendant can be observed in the MD simulations of methyl-substituted polyparaphenylene (*Figure 4*). Hopping between (8 GHz for H–T and 5 GHz for H–H) and oscillations within the preferred orientational states of the pendant ($\chi = 0, \pm 120$) are very similar for the H–H and H–T linkages. For both linkages, pendant rotations are independent of backbone and neighbouring pendant motion. Because pendant and backbone motion are not coordinated, discrete relaxations or first-order transitions associated with only the pendant may be expected. These pendant relaxations and transitions have been observed for many of the mono-alkyl, di-alkyl and alkoxy modified SPPPs[26].

In contrast, for class B pendants, steric interactions are so large that the pendant, as well as the backbone, is limited to discrete orientations separated by large potential energy barriers. Here, the trajectories between structural minima of the mer are intimately coupled to cooperative motion between the pendant and backbone and to bond distortions. This occurs for the phenyl and carbonyl-containing substituents where the lowest energy trajectories through the saddle points are a function of both χ and ϕ (*Figure 2c–e*). The intra-mer cooperativity necessitated by the class B pendants effectively increases the single-chain rigidity. The cooperativity coupled to the large rotational barriers and minimum number of accessible configurational states will result in very long chain relaxation times. Low-temperature relaxations associated with localized motion of the side-groups will be unlikely. For example, ^{2}H solid-state n.m.r. of pendant-deuterated poly(benzoyl paraphenylene) indicates that there is insufficient motion of the pendant at frequencies greater than 200 kHz and temperatures up to 100°C to reduce the deuterium quadrupole[47].

Because of the extended nature of the SPPP chain, bond angle fluctuations also become important factors contributing to chain flexibility and relaxation. Thermal excitation causes the average temporal bond angles (*Tables 4* and *5*) to be greater than those determined from structural minimizations. The extent of the bond angle fluctuations about the temporal average generally increases as the average angle increases. This is most noticeable for the H–T linkage of benzoyl-substituted paraphenylene. Although these fluctuations are smaller than reported in previous simulations of

Table 6 Characteristic ratio and persistence length for rigid-rod polymers

	C_∞	a (nm)	Ref.
PPP	434	93.0	
CH_3-PPP ($X = 0$)	428	91.4	
CH_3-PPP ($X = 0.5$)	352	75.2	
CH_3-PPP ($X = 1.0$)	298	63.7	
COC_6H_5-PPP ($X = 0$)	180	38.5	
COC_6H_5-PPP ($X = 0.5$)	69	14.9	
COC_6H_5-PPP ($X = 1.0$)	47	10.2	
PPP	102	22.0	23
trans-PBO	165	62.1	34
cis-PBO	147	64.8	34
cis-PBO	54	32.5	24
cis-PBZT	46	16.1	34
trans-PBZT	74	27.3	34
trans-PBZT	35	21.5	24

PPP, polyparaphenylene; CH_3-PPP, poly(methyl paraphenylene); COC_6H_5-PPP, poly(benzoyl paraphenylene); *cis*-PBO, poly(paraphenylene *cis*-benzobisoxazole); *trans*-PBO, poly(paraphenylene *trans*-benzobisoxazole); *cis*-PBZT, poly(paraphenylene *cis*-benzobisthiazole); *trans*-PBZT, poly(paraphenylene *trans*-benzobisthiazole)

polyparaphenylene[23], they are still sufficient to produce large fluctuations in persistence length. For example, the persistence length of a regioregular H–T chain can vary from 10 to 6 nm for backbone fluctuations from α_1 to $\alpha_1 + \delta_{\alpha 1}/2$ (see discussion below).

Characteristic chain parameters

The influence of regioregularity and pendant size on chain conformation can be quantified by comparing the characteristic ratio, C_∞, and persistence length, a, of polyparaphenylene, methyl-substituted polyparaphenylene and benzoyl-substituted polyparaphenylene. Calculation of these quantities must take into account the general orientational linkages (H–T, H–H, T–T, T–H) as well as the numerous configurational states of each linkage. Recall that the orientational dependence of each mer linkage is assigned to the mer preceding the linkage. As previously discussed, using this definition for a mer (*Figure 1*), MD results indicate that minimal correlation exists between neighbouring bond angles and lengths. Thus, C_∞ and a can be calculated using the RIS methodology outlined in equations (4)–(7).

The elements of the transformation matrix, $\langle \boldsymbol{T}_i \rangle$, are determined from the MD simulations and the symmetry of the backbone linkage. Since the orientational states of the mers (*Tables 4* and *5*) are symmetrically distributed about 0° and 180°, $\langle \sin \phi_i \rangle = 0$. For the class A pendants (H–T, T–T and H–H isomers of methyl-substituted paraphenylene) and T–T linkages (paraphenylene and the T–T isomer of benzoyl-substituted paraphenylene), the distribution is also symmetric about $-90°$ and $+90°$. In these cases, $\langle \cos \phi_i \rangle = 0$ and $\langle \boldsymbol{T}_i \rangle$ is greatly simplified. In contrast, intramer coupling between substituents in class B breaks the symmetry across $-90°$ and $+90°$ requiring $\langle \cos \phi_i \rangle$ for each isomeric state of the mer. This is the situation for the H–H and H–T isomers of benzoyl-substituted polyparaphenylene. Since there are insufficient statistics from the MD simulations to determine $\langle \cos \phi_i \rangle$, we determine $\langle \cos \phi_i \rangle$ at 300 K from the potential energy maps assuming Boltzmann statistics.

The elements of the statistical weight matrix, $\boldsymbol{U}_i$, are based on the relative potential energy of the configurational states of a linkage. Null values are included to exclude geometrically impossible combinations of mers, such as a contiguous series of H–H mers. To accommodate the relative contribution of various mers, the respective elements of the statistical weight matrix were multiplied by the relative fraction of each type of mer in the chain. From structural considerations it can be readily shown that the number of H–H and T–T mers in a chain must be equal to or differ by no more than one. Thus, the degree of regioirregularity can be quantified by the relative fraction of H–T mers, X.

Figure 5 shows the dependence of C_∞, determined at 300 K, on the relative fraction of H–T mers for methyl-substituted and benzoyl-substituted polyparaphenylene. A regioregular chain of H–T mers corresponds to $X = 1$ where as a regioregular chain of alternating H–H and T–T mers corresponds to $X = 0$. When $X = 0.5$, regioirregularity is maximized. C_∞ for polyparaphenylene ($C_\infty \sim 434$) is included for comparison (dashed line). This value is within the range of values determined from previous MM and MD simulations ($C_\infty \sim 100$–600)[23]. In all cases, $C_\infty < C_\infty$(PPP) and the end-to-end distance of the chain is less than the contour length. Since the asymmetric H–T mer accommodates the greatest distortion of the backbone, C_∞ is smallest for regioregular H–T chains and increases substantially as the fraction of symmetric H–H and T–T mers in the chain increases. Additionally, the magnitude of the characteristic parameters are very dependent on the degree of backbone distortion. For example, an increase of only 1° in the average backbone bond angle of polyparaphenylene will decrease the characteristic ratio, C_∞, by about 40% ($C_\infty(\alpha) \sim 434$, $C_\infty(\alpha + 1°) \sim 277$). When the pendant induces substantial out-of-plane bending, such as benzoyl, a fraction of the chain's configurational freedom is associated with the various torsional states. For example, with $\langle \cos \phi_i \rangle = 0$ for a regioregular H–T chain of benzoyl-substituted paraphenylene, C_∞ increases from 47 to 64.

Table 6 compares the persistence lengths and characteristic ratios determined for regioregular and regioirregular methyl-substituted and benzoyl-substituted polyparaphenylene with literature values determined from MD and MM simulations for other rigid-rod polymers. In contrast to the present MD simulations, those by Farmer *et al.*[23] included normal mode oscillations of the chain leading to a larger estimate of the average backbone distortion and thus smaller estimates of the characteristic parameters of the rigid-rod polymers (see p. 6023 footnote). In the case of PBO and PBZT, the benzobisoxazole and benzobisthiazole units are not ideally *para*, but the linkages are 5–15° from collinear[23,34]. This is the same degree of backbone distortion estimated for a benzoyl pendant and thus these polymers have similar characteristic ratios.

Solution measurements of a for SPPPs are difficult because of chain aggregation at very dilute solutions. However, the available data, such as dilute solution characterization of substituted paraphenylene with 67% sulfonate ester and 33% dodecyl pendants indicating $a \sim 10$–15 nm[14], agree favourably with the MM and MD results. Furthermore, recent small-angle neutron scattering experiments of poly(benzoyl paraphenylene) in the solid state estimated $a \sim 13$ nm[48], again agreeing favourably with the MM and MD results.

CONCLUSION

In general, the influence of the substituents on the isolated chain structure can be broadly distinguished based on the

degree of cooperativity for rotation about the paraphenylene linkage necessitated by the steric demands of the pendant. The conformation of poly(benzoyl paraphenylene) and other class B SPPPs can be described as a *thorny rod*. The steric demands of the pendants impede independent motion and thus the pendants resemble *thorns* distributed around the backbone. This contrasts long alkyl- and alkoxy-substituted polyparaphenylenes in which the pendant possesses substantial internal degrees of freedom and is described as a flexible *hair* (i.e. *hairy rod polymers*). Chain flexibility is restricted to tail–tail conformers associated with the asymmetric monomer unit and bond bending of the backbone phenyl linkages. The degree to which the chain deviates from linearity depends on the relative ratio of the H–H, H–T and T–T linkages and the associated distortions of the backbone bond angles necessary to accommodate the steric demands of the pendants

In the absence of strong associative interactions between pendants to overcome the large barriers to planar chain conformations, the solid-state conformations of these polymers are likely to resemble their single-chain conformations. Dihedral angles greater than ~40° effectively break conjugation along the backbone and have fundamental implications on the optical and electronic properties of these polymers. Large conjugation lengths are necessary for high electrical conductivities and will occur only in systems in which intermolecular forces and packing constraints overcome the intrachain repulsion between the *ortho* positions of the backbone rings. Thus SPPPs with very bulky, planar pendants and a high fraction of H–H or H–T linkages will exhibit large band gaps and low optical absorption. An increased fraction of symmetric T–T linkages could possible lead to an extended conjugation length and increased u.v.–vis absorption. This is consistent with previous u.v.–vis spectroscopic studies of poly(benzoyl paraphenylene)s with different fractions of H–T linkages[2]. Additionally, in the solid state, long relaxation times resulting from the large intramolecular barrier to motion may frustrate chain packing, leading to kinetically limited metastable states in the solid and melt.

ACKNOWLEDGEMENTS

This work was partially funded by the Air Force Office of Scientific Research and benefited from the central facilities of the Materials Directorate. The authors would like to thank M. Trimmer, T. Yeastes, D. Dean, G. Berry and B. Farmer for insightful discussions.

APPENDIX: DETAILED CALCULATION OF $\langle r^2\rangle_0$ and C_∞

The characteristic ratio is defined as the ratio of the mean square end-to-end distance of an unperturbed chain to the sum of the square of the individual bond lengths (equation (6)). For the specific case of the SPPPs considered here, the average length of a mer unit is nearly the same for all the states (*Tables 4* and *5*). Thus,

$$\sum_{i=1}^{n} l_i^2 = n\langle l\rangle^2 \tag{A1}$$

Following RIS formalism, the mean end-to-end distance is[42]

$$\langle r^2\rangle_0 = \tfrac{1}{Z}\mathcal{G}_1\mathcal{G}_2\cdots\mathcal{G}_n \tag{A2}$$

where

$$Z = \boldsymbol{U}_1\boldsymbol{U}_i^{n-2}\boldsymbol{U}_n \tag{A3}$$

$\boldsymbol{U}_1$, $\boldsymbol{U}_i$ and $\boldsymbol{U}_n$ are the statistical weight matrices for the first, internal and last mers, respectively. For ν potential states per mer, $\boldsymbol{U}_i$ is expressed in equation (5). U_1 and $\boldsymbol{U}_n$ are given by [42]

$$\boldsymbol{U}_1 = [\,1 \quad 0 \quad \cdots \quad 0\,] \tag{A4}$$

$$\boldsymbol{U}_n = \begin{bmatrix} 1 \\ 1 \\ \vdots \\ 1 \end{bmatrix} \tag{A5}$$

and where $\boldsymbol{U}_1$ and $\boldsymbol{U}_n$ have ν elements.

The weighted generator matrices, $\mathcal{G}_1$, $\mathcal{G}_i$ and $\mathcal{G}_n$ are for the first, internal and last mer, respectively, and given by[42]

$$\mathcal{G}_1[\,\boldsymbol{G}_1 \quad 0 \quad \cdots \quad 0\,] \tag{A6}$$

$$\mathcal{G}_i = \left(\boldsymbol{U}_i \otimes \boldsymbol{I}_{\mathrm{G}}\right)\|\boldsymbol{G}\|_i \quad 1 < i < n \tag{A7}$$

$$\mathcal{G}_n = \begin{bmatrix} \boldsymbol{G}_n \\ \boldsymbol{G}_n \\ \vdots \\ \boldsymbol{G}_n \end{bmatrix} \tag{A8}$$

Again for ν rotational states per mer, $\mathcal{G}_1, \mathcal{G}_i$ and $\mathcal{G}_n$ have dimensions $1 \times 5\nu$, $5\nu \times 5\nu$ and $5\nu \times 1$ respectively. $\boldsymbol{I}_{\mathrm{G}}$ denotes the identity matrix of same order as the unweighted generator matrices, $\boldsymbol{G}$, and $\otimes$ denotes a direct product. $\|\boldsymbol{G}\|_i$ represents the block diagonal matrix containing an unweighted generator matrix for each potential state of the mer. The ν generator matrices are arranged along the diagonal in the same sequence as the indexing of the columns of $\boldsymbol{U}_i$.

Finally, the unweighted generator matrices are expressed as[42]

$$\boldsymbol{G}_1 = \begin{bmatrix} 1 & 2\boldsymbol{l}^{\mathrm{T}}\langle\boldsymbol{T}\rangle & l^2 \end{bmatrix} \tag{A9}$$

$$\boldsymbol{G}_i = \begin{bmatrix} 1 & 2\boldsymbol{l}^{\mathrm{T}}\langle\boldsymbol{T}\rangle & l^2 \\ \boldsymbol{0} & \langle\boldsymbol{T}\rangle & \boldsymbol{l} \\ 0 & \boldsymbol{0} & 1 \end{bmatrix}_i \tag{A10}$$

$$\boldsymbol{G}_n = \begin{bmatrix} l^2 \\ \boldsymbol{l} \\ 1 \end{bmatrix} \tag{A11}$$

$\boldsymbol{l}$ is the virtual bond vector of the mer given in the local coordinates of the ith mer as $[l\ 0\ 0]$ where l is the virtual bond length. For the SPPPs, l is the same for all potential states of the ith mer. $\langle\boldsymbol{T}\rangle$ represents the transformation matrix given by equation (4). There is a different $\langle\boldsymbol{T}\rangle$ for each of the ν potential states of the ith mer.

From knowledge of the virtual bond length, bond angles and torsion angles of each potential state of the ith bond, the elements of $\boldsymbol{l}$ and $\langle\boldsymbol{T}\rangle$ are readily determined. For independent states, the elements of the statistical weight matrices can be deduced from the relative potential energies of each state, ε_i, assuming the probability of occupying each

state is related to a Boltzmann distribution, $w_{ij} \propto \exp(-\varepsilon_i/RT)$. Finally, C_∞ can be determined by sequentially calculating the ratio $\langle r^2\rangle_0/n\langle l\rangle^2$ for larger and larger n and extrapolating C_n *versus* $1/n$ to a limiting value as $1/n \rightarrow 0$.

REFERENCES

1. Marrocco, M., Trimmer, M., Hsu, L. and Gane', R., in *39th International SAMPE Conference*, 11 April 1994, p. 106.
2. Wang, Y. and Quirk, R., *Macromolecules*, 1995, **28**, 1872.
3. Kim, Y. H. and Webster, U. W., *J. Am. Chem. Soc.*, 1990, **112**, 4592.
4. Rehahn, M., Schülter, A.-D., Wegner, G. and Feast, W. J., *Polymer*, 1989, **30**, 1054.
5. Tour, J. M. and Stephens, E. B., *J. Am. Chem. Soc.*, 1991, **113**, 2309.
6. Percec, V., Okita, S. and Weiss, R., *Macromolecules*, 1992, **25**, 1816.
7. Yamamoto, T., Morita, A., Miyazaki, Y., Maruyama, T., Wakayama, H., Zhou, Z., Nakamura, Y., Kanbara, T., Sasaki, S. and Kubota, K., *Macromolecules*, 1992, **25**, 1214.
8. Stephens, E. B. and Tour, J. M., *Macromolecules*, 1993, **26**, 2420.
9. Chaturvedi, V., Tanaka, S. and Kaeriyama, K., *Macromolecules*, 1993, **26**, 2607.
10. Rau, I. U. and Rehahn, M., *Makromol. Chem.*, 1993, **194**, 2225.
11. Phillips, R. W., Sheares, V. V., Samulski, E. T. and DeSimone, J. M., *Macromolecules*, 1994, **27**, 2354.
12. Child, A. D. and Reynolds, J. R., *Macromolecules*, 1975, **1994**, 27.
13. Percec, V., Bae, J.-Y., Zhao, M. and Hill, D. R., *Macromolecules*, 1995, **28**, 6726.
14. Vanhee, S., Rukens, R., Lehmann, U., Rosenauer, C., Schulze, M., Köhler, W. and Wegner, G., *Macromolecules*, 1996, **29**, 5136.
15. Grob, M. C., Feiring, A. E., Auman, B. C., Percec, V., Zhao, M. and Hill, D. H., *Macromolecules*, 1996, **29**, 7284.
16. Percec, V., Zhao, M., Bae, J.-Y. and Hill, D. R., *Macromolecules*, 1996, **29**, 3727.
17. Tour, J. M., *Adv. Mater.*, 1994, **6**, 190.
18. Schülter, A.-D. and Wegner, G., *Acta Polym.*, 1993, **44**, 59.
19. Novak, B. M., Wallow, T. I., Goodson, F. and Loos, K., *Am. Chem. Soc. Polym. Div. Polym. Prepr.*, 1995, **36**, 693.
20. Cotts, P. M., Swager, T. M. and Zhou, Q., *Macromolecules*, 1996, **29**, 7323.
21. Connoly, M., Karasz, F. and Trimmer, M., *Macromolecules*, 1995, **28**, 1872.
22. Dean, D., Husband, M., Trimmer, M., *J. Poly. Sci.: Poly. Phys. Ed.*, 1998, in press.
23. Farmer, B. L., Chapman, B. R., Dudis, D. S. and Adams, W. W., *Polymer*, 1993, **34**, 1588.
24. Socci, E. P., Farmer, B. L. and Adams, W. W., *J. Polym. Sci., Part B: Polym. Phys.*, 1975, **1993**, 31.
25. Baker, K. N., Fratini, A. V., Resch, T., Knachel, H. C., Adams, W. W., Socci, E. P. and Farmer, B. L., *Polymer*, 1993, **34**, 1571.
26. Park, K. C., Dodd, L. R., Levon, K. and Kwei, T. K., *Macromolecules*, 1996, **29**, 7149.
27. Zhang, R. and Mattice, W. L., *Macromolecules*, 1995, **28**, 7454.
28. Trohalaki, S. and Dudis, D. S., *Makromol. Chem., Makromol. Symp.*, 1993, **65**, 163.
29. Vasudevan, V. J. and McGrath, J. E., *Macromolecules*, 1996, **29**, 637.
30. Trommsdorf, U. and Tomka, I., *Macromolecules*, 1995, **28**, 6128.
31. Trommsdorf, U. and Tomka, I., *Macromolecules*, 1995, **28**, 6138.
32. Depner, M. and Schürmann, B. L., *Polymer*, 1992, **33**, 398.
33. Jung, B. and Schürmann, B. L., *Macromolecules*, 1989, **22**, 477.
34. Zhang, R. and Mattice, W. L., *Macromolecules*, 1992, **25**, 4937.
35. Zhang, R. and Mattice, W. L., *Macromolecules*, 1993, **26**, 6100.
36. Maple, J. R., Hwang, M.-J., Stockfisch, T. P., Dinur, U., Waldmann, M., Ewig, C. S. and Hagler, A. T., *J. Comput. Chem.*, 1994, **15**, 162.
37. Dinur, U., Hagler, A. T., in *Review of Computational Chemistry*, Vol. 2., ed. K. B. Lipkowitz and D. B. Boyd. VCH, New York, 1991.
38. Waldman, M. and Hagler, A. T., *J. Comput. Chem.*, 1993, **14**, 1077.
39. Nosé, S. J., *Chem. Phys.*, 1984, **81**, 511.
40. Hoover, W. G., *Phys. Rev. A.*, 1985, **31**, 1695.
41. Pavlova, S. S. A., Ronova, I. A., Timofeeva, G. I. and Dubrovina, L. V., *J. Polym. Sci., Part B: Polym. Phys.*, 1993, **31**, 1725.
42. Mattice, W. L. and Suter, U. W., *Conformational Theory of Large Molecules*. Wiley, New York, 1994.
43. Cook, R., *Macrolmolecules*, 1961, **1987**, 20.
44. Mansfield, M. L., *Macromolecules*, 1983, **16**, 1863.
45. Tsuzuki, S. and Tanabe, K. J., *Phys. Chem.*, 1991, **95**, 139.
46. Dudis, D. S. and Vaia, R. A., unpublished results.
47. Vaia, R. A. and Cowen, B., manuscript in preparation.
48. Vaia, R. A., Benner, C., Krishnamoorti, R. and Trimmer, M., *J. Poly. Sci.: Poly. Phys. Ed.*, submitted.